Journal of Magnetic Resonance 205 (2010) 102–108

Contents lists available at ScienceDirect

Journal of Magnetic Resonance

journal homepage: www.elsevier.com/locate/jmr

Simulation studies of instrumental artifacts on spin $I = 1$ double quantum filtered NMR spectroscopy

Cheng Sun, Gregory S. Boutis *

Brooklyn College, Department of Physics, 2900 Bedford Avenue, Brooklyn, NY 11210, United States

ARTICLE INFO

Article history:
Received 3 February 2010
Revised 8 April 2010
Available online 24 April 2010

Keywords:
Double quantum filtered NMR
Quadrupolar interaction
Deuterium
Multiple quantum coherence

ABSTRACT

We report on the results of a simulation based study of the effect of various experimental artifacts for spin $I = 1$ double quantum filtered NMR. The simulation captures the effects of static field inhomogeneity, finite pulse widths, phase errors, transients and radio frequency field inhomogeneity. We simulated the spectral distortions introduced under these errors for four, eight and sixteen step phase cycles that are well known in the NMR community. The dominating pulse errors are radio frequency field inhomogeneity and antisymmetric pulse transients. These errors result in the reduction of signal intensity as well as an introduction of distortions in the detected double quantum filtered spectrum. Using the simulation tool we studied the improvement one obtains when implementing a sixteen step phase cycle over a four step phase cycle. The results indicate that implementing a sixteen step phase cycle over an eight or four step phase cycle does not result in a significant reduction in the DQF intensity loss, or reduction in spectral distortions for antisymmetric transients.

1. Introduction

The local ordering of water in many biological systems is known to play a critical role in structure and function. Among various methods, deuterium double quantum filtered (DQF) nuclear magnetic resonance (NMR) is a powerful experimental scheme for characterizing anisotropic motion of nuclear spins resulting from local ordering [1]. The method has been implemented with great success in a wide range of systems. For example, the technique has been used to study motional anisotropy of water in blood vessels [2], the dynamics of water in tendon [3], the interaction of water within a purple membrane suspension [4], to detect anisotropy in cartilage [5,6] and to discriminate between various compartments in sciatic nerve [7]. More recently the experimental scheme has been applied to study spinal disc degeneration [8]. A review of recent achievements in DQF NMR is given in Ref. [9].

Bodenhausen, Kogler and Ernst proposed a general procedure to design phase cycles that select desirable coherence transfer pathways while suppressing undesired pathways [10]. To date, various phase cycling schemes have been developed to select double quantum coherence while suppressing single and zero quantum coherence pathways. The pulse sequence shown in Fig. 1 is an example of a commonly implemented sequence that allows for detecting double quantum coherence while suppressing single and zero quantum pathways for spin $I = 1$ [2,11]. Under perfect experimental conditions the real component of the DQF spectrum is dispersive. However, it is not uncommon to detect a distorted, slightly asymmetric line shape in experiments. Such spectral distortions make analysis of DQF spectra challenging, in particular the determination of the residual quadrupolar coupling. In part, the purpose of this work is to investigate the source of these distortions by numerical simulation.

Pulse phase cycling is a well known method to minimize the effects of instrumental artifacts in a variety of NMR experiments. For example, the cyclically ordered phase sequence (CYCLOPS) is commonly implemented to suppress quadrature images in single pulse experiments [12]. As a second example, the EXORCYCLE is often used to compensate for imperfect 180° pulses in spin-echo sequences [13]. To date there have been numerous reports for enhancing multiple quantum filtering that involve a variety of experimental schemes. For instance, it was shown by Kumar that a variation in the pulse flip angle allows for distinguishing between various classes and types of transitions in two-dimensional multiple quantum NMR spectroscopy [14]. An estimate of coherence transfer leakage as a function of flip angle error was reported by Jerschow [15] and a phase cycling scheme was recently proposed by Bachert for reducing static field inhomogeneity effects in triple quantum filtered sodium MRI [16]. A very useful, and now commonly used scheme for enhancing signal to noise involves implementing a π pulse in the conventional DQF sequence to refocus static field inhomogeneity [9]. Multiple quantum filtering can also be performed via RF gradients as shown by Chuang and Cory [17].

* Corresponding author. Fax: +1 718 951 4407.
E-mail address: gboutis@brooklyn.cuny.edu (G.S. Boutis).

1090-7807/$ - see front matter © 2010 Elsevier Inc. All rights reserved.
doi:10.1016/j.jmr.2010.04.008

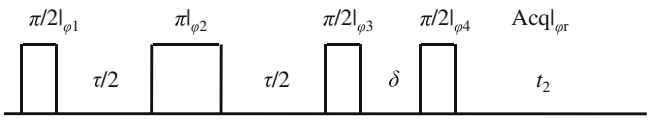

Fig. 1. A four pulse DQF RF pulse sequence for generating and detecting double quantum coherence used in this work.

In this work, we report on the results of a simulation based study of the effects of a variety of instrumental artifacts on spin $I = 1$ DQF NMR spectroscopy. We also investigate the improvement in suppressing these unwanted distortions when implementing an already known sixteen step phase cycling scheme compared to four or eight step cycles.

2. Simulation

The spin $I = 1$ DQF NMR spectra were simulated based on the pulse sequence shown in Fig. 1. Referring to Fig. 1, τ is the creation time of double quantum coherence and δ is the double quantum evolution time. Generally, δ is set to be a few μs to minimize signal loss due to $T_{2,DQ}$. After the second 90° pulse double quantum coherence is created and it is then detected by applying a third 90° pulse whereby the ±2 quantum coherence is transformed to −1 quantum coherence for detection by a quadrature receiver [18]. The 180° pulse in the sequence is utilized to refocus signal loss caused by static field inhomogeneity [9]. In practice, the phases of all the pulses are cycled to suppress zero and single quantum coherence. In this work we simulated the four, eight, and sixteen step DQF phase cycles that are well known in the NMR community and are tabulated in Tables 1–3 respectively.

All simulations were carried out using Matlab. In our model, the residual quadrupolar coupling constant was set to $\delta_{zz} = 133$ Hz, the spin–spin lattice relaxation, T_2, was 3 ms, τ was 2 ms and δ was 10 μs. It should be noted that the parameters were chosen as they are close to values reported in the existing literature [2,8]. A dwell time of 500 μs was used and for each spectrum an acquisition time of 250 ms was simulated. In our study we assumed that the quadrupolar interaction is usually much larger than the dipolar interaction and we have omitted the latter from our simulation. For the purpose of the simulation we assumed a distribution of 50 spins at different angles θ for the quadrupolar interaction defined below.

In a large and static magnetic field the quadrupolar interaction is much smaller than the Zeeman interaction. In this limit the secular approximation to the first order quadrupolar interaction is appropriate and is given by [19,20]

$$\widehat{H_q} = \omega_q(3\widehat{I_z}^2 - \widehat{I}\cdot\widehat{I}) \tag{1}$$

where I is the angular momentum of the spin and ω_q is the quadrupolar frequency which is given by

$$\omega_q = \frac{1}{2}\delta_{zz}[3\cos^2\theta - 1] - \eta\cos(2\varphi)\sin(\theta) \tag{2}$$

Table 1
A four step phase cycling scheme for detecting double quantum coherence for spin $I = 1$ species. The phase cycle suppresses single and zero quantum coherence and allows for detecting only double quantum coherence created during time δ shown in Fig. 1.

Step no.	ϕ_1	ϕ_2	ϕ_3	ϕ_4	ϕ_r
1	x	y	x	x	x
2	x	y	x	y	$-y$
3	x	y	x	$-x$	$-x$
4	x	y	x	$-y$	y

Table 2
An eight step phase cycling scheme for detecting double quantum coherence for spin $I = 1$ species. The phase cycle suppresses single and zero quantum coherence and allows for detecting only double quantum coherence created during time δ shown in Fig. 1.

Step no.	ϕ_1	ϕ_2	ϕ_3	ϕ_4	ϕ_r
1	x	y	x	x	x
2	x	y	x	y	$-y$
3	x	y	x	$-x$	$-x$
4	x	y	x	$-y$	y
5	$-x$	y	x	x	$-x$
6	$-x$	y	x	y	y
7	$-x$	y	x	$-x$	x
8	$-x$	y	x	$-y$	$-y$

Table 3
A sixteen step phase cycling scheme for detecting double quantum coherence for spin $I = 1$ species. The phase cycle suppresses single and zero quantum coherence and allows for detecting only double quantum coherence created during time δ shown in Fig. 1.

Step no.	ϕ_1	ϕ_2	ϕ_3	ϕ_4	ϕ_r
1	x	y	x	x	x
2	x	y	x	y	$-y$
3	x	y	x	$-x$	$-x$
4	x	y	x	$-y$	y
5	$-x$	y	x	x	$-x$
6	$-x$	y	x	y	y
7	$-x$	y	x	$-x$	x
8	$-x$	y	x	$-y$	$-y$
9	y	y	x	x	$-y$
10	y	y	x	y	$-x$
11	y	y	x	$-x$	y
12	y	y	x	$-y$	x
13	$-y$	y	x	x	y
14	$-y$	y	x	y	x
15	$-y$	y	x	$-x$	$-y$
16	$-y$	y	x	$-y$	$-x$

In the above expression θ and φ are the usual Euler angles with respect to the static magnetic field and η is the asymmetry parameter. The quadrupolar coupling constant δ_{zz} is given by

$$\delta_{zz} = \frac{3eQ}{4I(2I-1)}V_{zz} \tag{3}$$

where e is the charge of the proton, Q is the electric quadrupolar moment of the nucleus and V_{zz} is the component of the electric field tensor along the azimuth [19]. It should be noted that in this work we assumed the asymmetry parameter $\eta = 0$ for simplicity.

Given the spin operators for $I = 1$ proposed by Vega and Pines [21] Eq. (1) may be written as

$$\widehat{H_q} = 2\omega_q(I_{x,3} - I_{y,3}) \tag{4}$$

where $I_{x,3} = \frac{1}{2}(\widehat{I_z}^2 - \widehat{I_y}^2)$ and $I_{y,3} = \frac{1}{2}(\widehat{I_x}^2 - \widehat{I_z}^2)$ defined in [21].

The Hamiltonian for an RF pulse, $\widehat{H_{RF}}$, may be written as

$$\widehat{H_{RF}} = \omega_{nut}[\widehat{I_x}cos(\phi_0) + \widehat{I_y}sin(\phi_0)] \tag{5}$$

where ϕ_0 is the phase of the RF pulse. By convention $\phi_0 = 0$ for an x pulse and $\phi_0 = 90°$ for a y pulse. The nutation frequency, ω_{nut}, is given by the expression

$$\omega_{nut} = \frac{\beta_p}{\tau_p} \tag{6}$$

where β_p is the flip angle and τ_p is the RF pulse width.

Beginning with spins at equilibrium in the high temperature approximation, the density matrix is given by $\widehat{\rho}(0) = \widehat{I_z}$. Following the pulse sequence in Fig. 1 the evolution of the density matrix was

computed under any corresponding Hamiltonian by the solution to the Von Neumann equation

$$\hat{\rho}(t_2) = exp[-i\hat{H}(t_2 - t_1)]\hat{\rho}(t_1)exp[i\hat{H}(t_2 - t_1)] \quad (7)$$

where t_1 and t_2 are two consecutive time periods.

The spin operator for a receiver with a phase $\phi_r = x$ is given by $\hat{I}_r = \hat{I}_x + i\hat{I}_y$, and $\hat{I}_r = \hat{I}_y - i\hat{I}_x$ for a receiver with a phase of $\phi_r = y$. Therefore the NMR signal, $S(t)$, as a function of time may be simulated by computing

$$S(t) = Trace[\hat{I}_r\hat{\rho}(t)] \quad (8)$$

For any given phase cycle the NMR signal arising from each step was simulated individually and the final signal was determined by superposition of the cycles.

3. Results and discussion

In this work we studied the effects of (1) static field inhomogeneity, (2) errors in the phase of RF pulses, (3) finite pulse widths effects, (4) RF pulse inhomogeneity and (5) symmetric and anti-symmetric RF transients on the DQF spectrum.

(1) Static field inhomogeneity.

A gradient in the magnetic field results in a distribution of Larmor frequencies distributed spatially across the sample. In the rotating frame the Hamiltonian for the static field, $\widehat{H_z}$, is given by

$$\widehat{H_z} = \omega_0(z)\hat{I}_z \quad (9)$$

where $\omega_0(z)$ is the difference between the Larmor frequency and the frequency that a spin at position z experiences. In this work, a linear distribution for $\omega_0(z)$ ranging from $-\Delta B_0$ to ΔB_0 along z-axis was assumed using 31 slices. The parameter for modeling the inhomogeneity, ΔB_0, was varied from 0 to 20 Hz. The variation in the DQF peak intensity as a function of ΔB_0 is shown in Fig. 2.

(2) Errors in the relative phases of RF pulses.

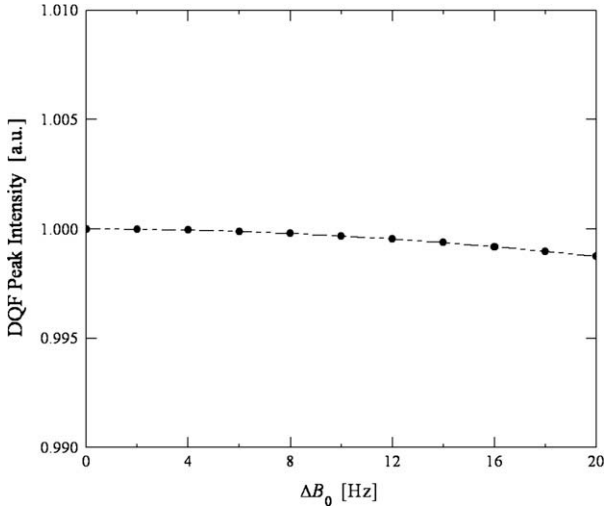

Fig. 2. Imaginary part of the DQF peak intensity as a function of Δ B_0. The parameter ΔB_0 characterizes the extent of static field inhomogeneity as discussed in the text. The DQF peak intensity was determined by measuring the intensity at $\omega = 0$ of the DQF spectrum simulated by using the four step phase cycle tabulated in Table 1. The dashed line is intended to guide the eye and does not represent or intend to be a fit to the data.

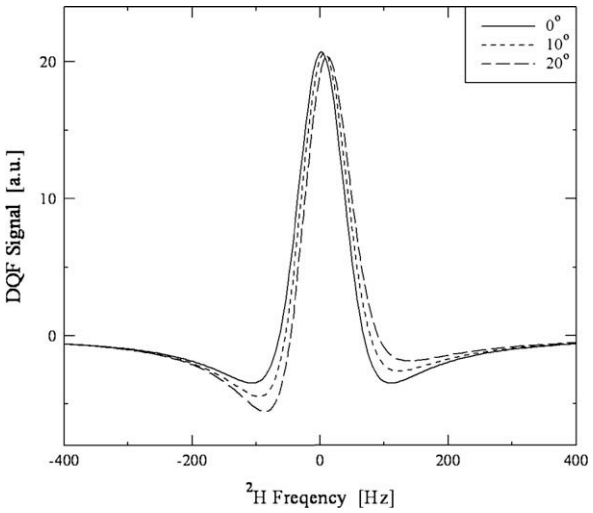

Fig. 3. Imaginary part of the DQF spectra simulated with errors in RF pulse phase, $\phi_p = 0°$, 10° and 20°. The four step phase cycle tabulated in Table 1 was implemented in the simulation of the spectra shown.

Given by Eq. (5), the Hamiltonian for an x pulse is $\widehat{H_{RF}}^x = \omega_{nut}\hat{I}_x$. Relative to the x-axis, we consider phases errors in the y, $-y$, and $-x$ axes. The Hamiltonian for a y pulse, for example, is given by the expression

$$\widehat{H_{RF}}^y = \omega_{nut}[\hat{I}_x cos(\phi_p + 90°) + \hat{I}_y sin(\phi_p + 90°)] \quad (10)$$

For simplicity we assume the phase errors between x and $-x$ or $-y$ pulse are the same. Thus, the Hamiltonians for $-x$ or $-y$ pulses are given by

$$\widehat{H_{RF}}^{-x} = \omega_{nut}[\hat{I}_x cos(\phi_p + 180°) + \hat{I}_y sin(\phi_p + 180°)] \quad (11)$$

$$\widehat{H_{RF}}^{-y} = \omega_{nut}[\hat{I}_x cos(\phi_p + 270°) + \hat{I}_y sin(\phi_p + 270°)] \quad (12)$$

With the Hamiltonians above, the simulations were carried out for different values of ϕ_p ranging from 0 to 20°. The simulated DQF spectra and the measured peak intensities are shown in Figs. 3 and 4 respectively. It is worth noting that the phase error ϕ_p can

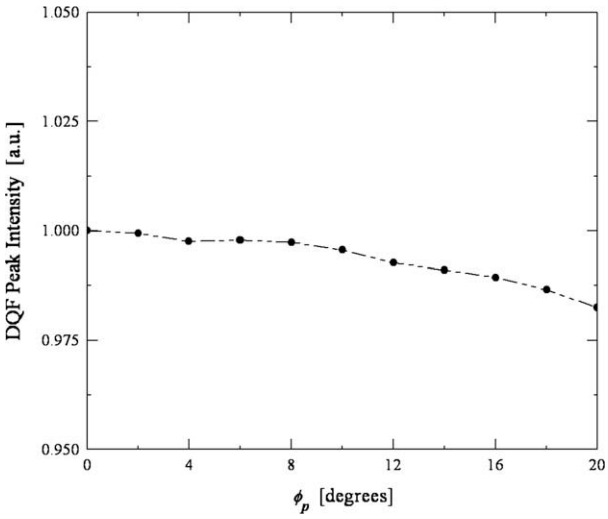

Fig. 4. Imaginary part of the DQF peak intensity as a function of the errors in RF pulse phases, ϕ_p. The DQF peak intensity was determined by measuring the intensity at $\omega = 0$ of the DQF spectrum simulated by using the four step phase cycle tabulated in Table 1. The dashed line is intended to guide the eye and does not represent or intend to be a fit to the data.

be characterized by a stroboscopically detected $[\tau_1,(\pi/2)_x,2\tau_1,(\pi/2)_y,\tau_1]^n$ sequence, where τ_1 is the time between two consecutive pulses and n is the number of loops [22].

(3) Finite pulse widths effects.

Normally if the RF pulse width, τ_p, is very short the evolution under the quadrupolar interaction may be neglected. In practice, under conditions of weak RF power, one cannot ignore the composite evolution of the quadrupolar and RF Hamiltonians during the pulses. The composite evolution may result in distortions in the detected DQF spectrum. For comparison we studied two situations; a simulated DQF spectrum that does not account for the quadrupolar evolution during the pulse, and one that accounts for both $\widehat{H_{RF}}$ and $\widehat{H_q}$ during the RF irradiation. For each model, simulations were performed for pulse width values ranging from 1 to 10 μs. The variation in the DQF peak intensity for both simulations is given in Fig. 5.

(4) RF pulse inhomogeneity.

In realistic situations of inhomogeneous RF fields not all the spins of a sample experience the same flip angle. This therefore causes a loss in NMR signal compared with a spatially homogeneous RF field. The degree of inhomogeneity can be characterized by the ratio of the NMR signal intensity after a 450° pulse to that after a 90° pulse, i.e. I^{450}/I^{90} [23]. In our simulation a Gaussian distribution of flip angles was implemented as follows

$$\omega^i_{nut} = \frac{\beta_p}{\tau_p} exp[-\alpha x_i^2] \tag{13}$$

In the above expression α is a coefficient that characterizes the degree of inhomogeneity in the ith slice. The case $\alpha = 0$ is for a homogeneous RF field, x_i is the coordinate along the x-axis and was assumed to be linearly distributed and set to 31 slices. The Hamiltonian for the RF pulse in the ith slice is then given by

$$\widehat{H^i_{RF}} = \omega^i_{nut}[\widehat{I^i_x} cos(\phi_0) + \widehat{I^i_y} sin(\phi_0)] \tag{14}$$

To compute the DQF spectra we performed the evolved density matrix under the pulse sequence shown in Fig. 1., in each RF slice. The total DQF spectra was then determined by superposition of the 31 slices. In our simulation we varied α from 0 to 2 (corresponding to a ratio, I^{450}/I^{90} = 1 to 0.49), the resulting DQF spectra are shown in Fig. 7. Fig. 6 shows the correlation between the parameter α and I^{450}/I^{90}. The data shown in Fig. 6 were determined by a simulation of a single pulse under the conditions of RF inhomogeneity for different values of α. The DQF peak intensity as a function of I^{450}/I^{90} is shown in Fig. 8.

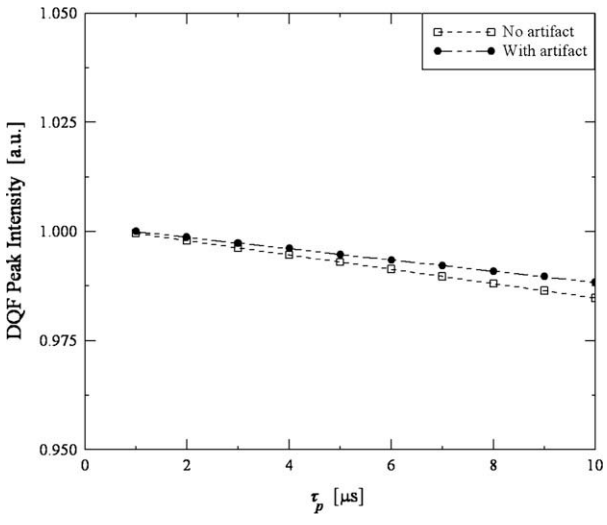

Fig. 5. Imaginary part of the DQF peak intensity at $\omega = 0$ as a function of the RF pulse width, τ_p. Open squares represent the DQF peak intensity simulated without considering the effect of finite pulse widths and filled circles show the results simulated with the effect of finite pulse widths. Both simulations used the four step phase cycle tabulated in Table 1. The dashed lines are intended to guide the eye and do not represent or intend to be a fit to the data.

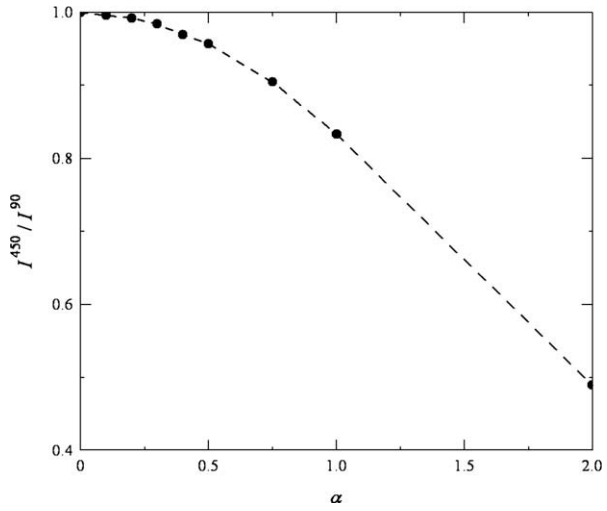

Fig. 6. The correlation of the parameter α which was used to model the RF inhomogeneity, defined by Eq. (13), and the ratio of signal intensity for a 450° pulse to a 90° pulse, I^{450}/I^{90}, that can be experimentally determined. The dashed line is intended to guide the eye and does not represent or intend to be a fit to the data.

(5) Symmetric and antisymmetric RF transients.

For a pulse applied along the x-axis an RF transient may exist that may be modeled by y-phase RF irradiation that may occur before and after the x pulse. If the phases of these artifacts are the same, i.e. y and y, the distortion is termed a symmetric transient. If the phases are opposite, i.e. y and $-y$, the distortion is known as an antisymmetric transient [22]. In this work the Hamiltonians for these artifacts are modeled by the following expressions

$$\widehat{H^b_{RF}} = \omega_{nut}[\widehat{I_x} cos(\phi_0 + 90^\circ) + \widehat{I_y} sin(\phi_0 + 90^\circ)] \tag{15}$$

$$\widehat{H_{RF}} = \omega_{nut}[\widehat{I_x} cos(\phi_0) + \widehat{I_y} sin(\phi_0)] \tag{16}$$

$$\widehat{H^a_{RF}} = \pm\omega_{nut}[\widehat{I_x} cos(\phi_0 + 90^\circ) + \widehat{I_y} sin(\phi_0 + 90^\circ)] \tag{17}$$

The definition of the time durations of the Hamiltonians for any given pulse are as follows:

$$\begin{aligned} &0 < t < \varepsilon\tau_p \quad \widehat{H^b_{RF}} \\ &\varepsilon\tau_p < t < \tau_p + \varepsilon\tau_p \quad \widehat{H_{RF}} \\ &\tau_p + \varepsilon\tau_p < t < \tau_p + 2\varepsilon\tau_p \quad \widehat{H^a_{RF}} \end{aligned} \tag{18}$$

The model that we are implementing for the phase transients is similar to that used by Vega in studies of phase-modulated multiple-pulse sequences for homonuclear decoupling in solid-state proton NMR [24]. In the above expressions $\widehat{H^b_{RF}}$ and $\widehat{H^a_{RF}}$ model the transient artifacts before and after the main pulse that is given by $\widehat{H_{RF}}$. The parameter $\varepsilon\tau_p$ above is a constant that determines the duration that the RF transient is on, and in our model the ± sign in front of H^a_{RF} determines if the transients are symmetric or antisymmetric. It should be noted that effects of RF transients may be experimentally characterized by a flip-flop sequence by measuring a parameter J_1 [25,26]. The relation between J_1 and ε in our model is given by average Hamiltonian theory as follows [25]:

$$J_1 = -\varepsilon\omega_{nut}\tau_p = -\varepsilon\pi/2 \tag{19}$$

The first order term of the Magnus expansion for the antisymmetric transients for our model in the flip-flop sequence is given by

$$H_T^0 = J_1/\tau_c(I_{z,1} - I_{y,1}) \tag{20}$$

It should be pointed out that the model for the RF transients is different from that used in the work by Rhim et al. [25]. The assumption in their work was that the RF transients were on throughout the entire pulse, whereas our model assumes the transients are on before and after the main RF pulse. For simplicity we assumed that the amplitude of the RF transients are same as the main pulse itself. In our simulation, the π pulse had twice the intensity of a $\pi/2$ pulse and the duration of the π pulse was kept the same as that of a $\pi/2$ pulse. The transients for the π pulse, in our model, were also double in intensity compared to a $\pi/2$ pulse. The time duration of the transients in both cases of a π and $\pi/2$ pulse are kept the same. The assumptions of this model are justified if one were to experimentally tune a π pulse relative to a $\pi/2$ pulse by varying the RF power, rather than the time duration of the pulse. We simulated both symmetric and antisymmetric transients with ε ranging from 0 to 0.2. The measured DQF intensity from both symmetric and antisymmetric cases are plotted in Fig. 9 as a function of ε. The DQF spectra simulated from the antisymmetric RF transients are shown in Fig. 10.

We highlight the spectral distortions introduced by the above artifacts by providing examples of the imaginary component of the DQF spectra as well as the intensity from the imaginary component at $\omega = 0$. Fig. 2 shows that the change in the DQF peak intensity is within 0.2 percent when the static field inhomogeneity, ΔB_0, is as large as 20 Hz. Fig. 4 reveals that the change in the intensity is less than 2 percent even when the phase error between x- and y-pulses is as much as 20°. Fig. 5 highlights that the change in intensity due to finite pulse width effects. The simulation indicates the difference is only 0.3 percent when τ_p is as long as 10 μs. It is clear from Figs. 2, 4 and 5 that the effects of the above three artifacts on the DQF signal appear to be negligible.

Referring to Fig. 3 a distorted DQF spectrum is observed once a phase error is introduced. Although the distortion is small it becomes evident when $\phi_p = 20°$. These results show that phase error artifacts can change the line shape of the DQF spectrum. As discussed below, compared with artifacts (4) and (5) the degree of the distortion appears to be fairly small. It is worth noting that the DQF spectra simulated with artifacts (1) and (3) do not show a significant spectral distortion and are not shown.

Fig. 7 shows the DQF spectra simulated by varying the RF inhomogeneity parameter, I^{450}/I^{90}, from the four step phase cycle. As the inhomogeneity increases, apart from the decrease in intensity, a small distortion in the DQF line shape is also observed. It should be pointed out that the distortion shown in the figure cannot be corrected by phasing the data. Referring to Fig. 7, the signal intensities from the four step phase cycle are indicated in filled circles in Fig. 8. Comparing the intensities measured at the homogeneous condition, i.e. $I^{450}/I^{90} = 1$, and at a grossly inhomogeneous case, i.e. $I^{450}/I^{90} = 0.49$, the DQF signal is decreased by approximately 33 percent. This reveals that the RF pulse inhomogeneity can reduce the DQF signal substantially.

In Fig. 9 we show the results of the four step DQF phase cycle simulation for symmetric and antisymmetric transients. In Fig. 9 at $\varepsilon = 0.2$, the intensity change for symmetric transients is approximately only 20 percent. However, for antisymmetric transients at any given value of ε the DQF peak intensity loss is much larger. For example, at $\varepsilon = 0.2$ the loss in signal intensity is 110 percent for antisymmetric transients. Thus antisymmetric transients appear to have a more significant effect. It should be pointed out that the metric used for measuring peak intensity involves taking the

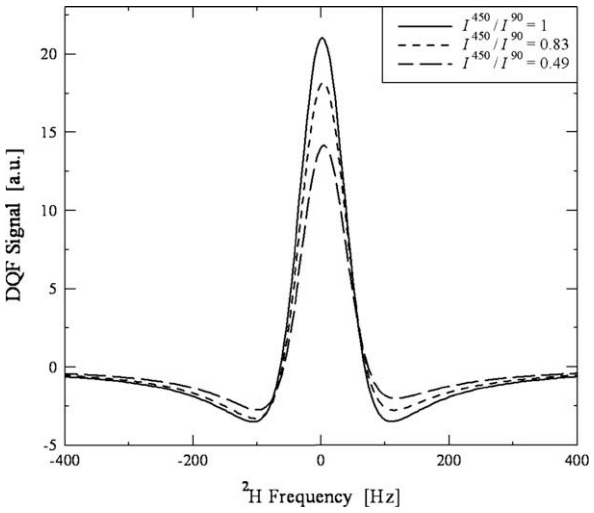

Fig. 7. Imaginary part of the DQF spectra simulated with RF pulse inhomogeneity artifacts, $I^{450}/I^{90} = 1$, 0.83, 0.49. The four step phase cycle tabulated in Table 1 was implemented in the simulation of the spectra shown. The distortion shown cannot be corrected by phasing the data.

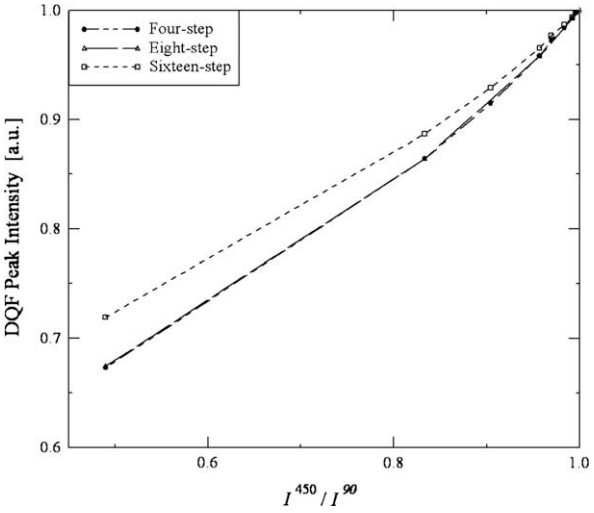

Fig. 8. Imaginary part of the DQF peak intensity at $\omega = 0$ as a function of I^{450}/I^{90}, a parameter that characterizes the RF inhomogeneity as described in the text. The result of using the four step phase cycle are indicated with filled circles, open triangles for the eight step cycle and open squares for sixteen step phase cycle. The dashed lines are intended to guide the eye and do not represent or intend to be a fit to the data. The data have all been normalized for the different phase cycling schemes to the intensity when no artifact is present (i.e. $I^{450}/I^{90} = 1$).

value at $\omega = 0$. In some cases the transients result in a large distortion of the spectra such that the signal intensity becomes negative at $\omega = 0$. Examples of the corresponding spectral distortions for the case of antisymmetric transients are shown in Fig. 10. Referring to Fig. 10, the simulation results show that there is a τ dependence in the spectral distortion. Our results show the DQF spectra for $\tau = 2$ ms and $\tau = 6$ ms. For example, when $\varepsilon = 0.16$ the shape of the spectra is much different at the two different τ values that we studied. Careful examination of the spectra, particularly at $\varepsilon = 0.16$ for $\tau = 6$ ms, reveals that the distortion cannot be corrected by phasing the data. The shape of the spectra will depend on the strength of the residual quadrupolar coupling constant, which gives a different τ dependence in the DQF spectra. It should be pointed out that if a system contains a distribution of environments with different quadrupolar coupling constants that the

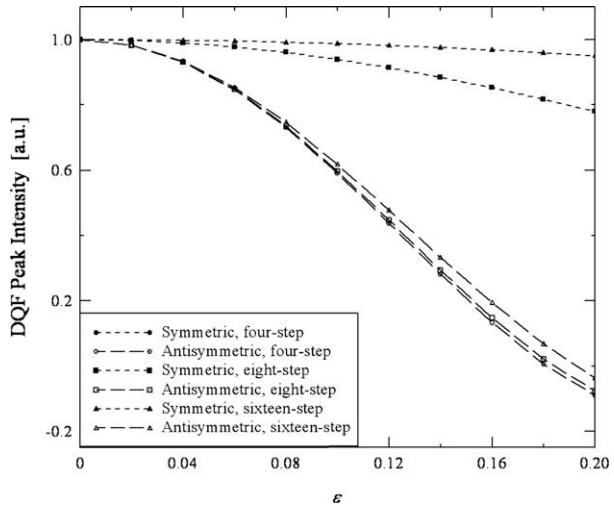

Fig. 9. Imaginary part of the DQF peak intensity at $\omega = 0$ as a function of ε, as described in the text. Filled marks indicate the results simulated with symmetric RF pulse transients and open marks for antisymmetric transients. The results of using the four step phase cycle are shown as circles, squares for eight step cycle and triangles for the sixteen step phase cycle. The dashed lines are intended to guide the eye and do not represent or intend to be a fit to the data. The symbols of symmetric four step cycle (filled circles) are obscured by those of symmetric eight step cycle (filled squares).

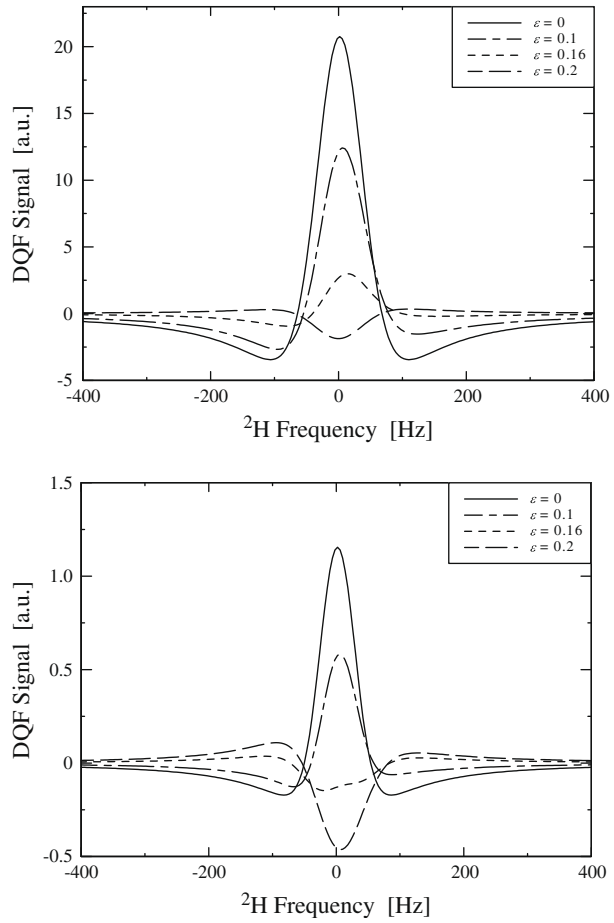

Fig. 10. Imaginary part of the DQF spectra simulated with four antisymmetric transient conditions, $\varepsilon = 0$, 0.1, 0.16 and 0.2 as described in the text. The four step phase cycle tabulated in Table 1 was implemented in the simulation of the spectra shown for Top. $\tau = 2$ ms and Bottom. $\tau = 6$ ms. The results show a decrease in DQF intensity and a spectral distortion as the transients increase and are dependent on τ.

DQF spectra may be further distorted due to the superposition of the individual DQF signals.

In summary, from the simulations using the four step DQF phase cycle, we found the effects of RF pulse inhomogeneity and transients on the DQF spectrum are dominant. We performed a similar simulation using the eight and sixteen step phase cycles given in Tables 2 and 3 and describe the results of this simulation below.

Fig. 8 shows that the eight step phase cycle produces similar results as the four step phase cycle when considering RF inhomogeneity effects. By implementing the sixteen step phase cycle over the eight or four step phase cycle the effects of RF pulse inhomogeneity on the DQF signal appear to be reduced. The simulation results reveal that one may enhance the signal intensity by approximately 5 percent when applying a sixteen step phase cycle over a four step phase cycle with grossly inhomogeneous RF fields.

Fig. 9 highlights results from the eight step phase cycle and sixteen step phase cycle for symmetric and antisymmetric phase transients. For the four step phase cycle the reduction of the DQF intensity from $\varepsilon = 0$ to $\varepsilon = 0.2$ is measured to be 20 percent for symmetric transients and 110 percent for antisymmetric transients. For the eight and sixteen step phase cycles they are approximately the same. From these results two trends are clear. First, the effect of antisymmetric transients are again greater than that of symmetric transients for any given phase cycling scheme. Second, for the same type of RF transients the sixteen step phase cycle does not do significantly better at minimizing the signal intensity loss compared to the four step phase cycle.

As discussed above, the DQF line shape was also effected by the phase cycle. To further investigate these distortions, DQF spectra simulated with the four and sixteen step phase cycles are presented in Figs. 10 and 11. Fig. 11 shows the simulation results for antisymmetric transients with $\varepsilon = 0$, 0.1, 0.16 and 0.2 using the sixteen step phase cycle. Comparing Figs. 11 and 10, there are some differences in the preservation of the symmetry of the line shape by implementing the sixteen step phase cycle over the four step phase cycle. These differences are not clearly evident from Fig. 9, that only shows the DQF peak intensity at $\omega = 0$. For $\varepsilon = 0.2$ for example, the four step phase cycle spectrum is skewed whereas the spectrum for the sixteen step phase cycle is also skewed, but differently. Fig. 12 shows the spectra simulated with the four, eight

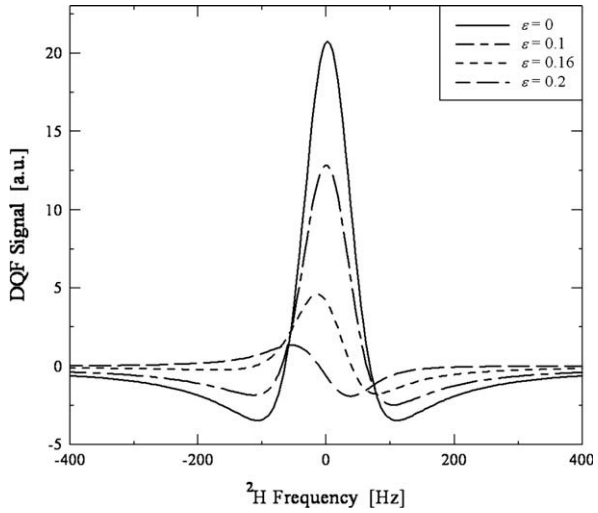

Fig. 11. Imaginary part of the DQF spectra simulated with four antisymmetric transient conditions, $\varepsilon = 0$, 0.1, 0.16 and 0.2 as described in the text. The sixteen step phase cycle tabulated in Table 3 was implemented in the simulation of the spectra shown. The results show a decrease in DQF intensity and a distortion of spectral line shape as the transients increase.

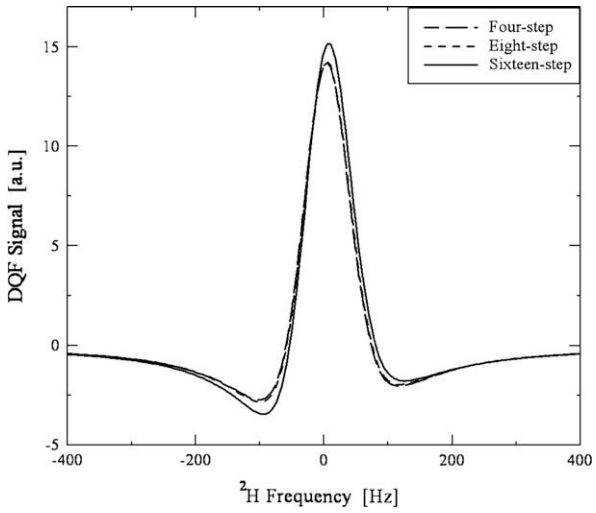

Fig. 12. Imaginary part of the DQF spectra simulated with an RF pulse inhomogeneity artifact of $I^{450}/I^{90} = 0.49$. The four, eight, and sixteen step phase cycles tabulated in Tables 1–3 were implemented respectively in the simulation of the spectra shown.

and sixteen step phase cycles under a gross RF inhomogeneity of $I^{450}/I^{90} = 0.49$. The results show that the spectral distortion is almost the same for all three phase cycles and therefore unlike the results obtained from RF transient artifacts. These results indicate that the line shape distortions arising from RF inhomogeneity effects are not sensitive to the three phase cycles we examined.

4. Conclusion

In this work we report on the effects of field inhomogeneity and a variety of pulses artifacts on spin $I = 1$ DQF NMR by simulation. Our results indicate that in the limiting case of a weak residual quadrupolar interaction, which is commonly encountered in DQF experiments, the static magnetic field inhomogeneity, phase errors and finite pulse width effects are negligible. However, RF pulse inhomogeneity and transients are two artifacts that cause a substantial loss in the DQF signal intensity as well as significant spectral distortions. For RF pulse transients, the effects of antisymmetric transients are greater than that of symmetric transients. We also simulated the potential improvement one obtains by implementing an eight and sixteen step phase cycling scheme when RF pulse inhomogeneity and transients are present. It is expected that reduction in spectral distortions may be achieved by applying more advanced phase cycling schemes or by constructing symmetric cycles that remove unwanted pulse distortions to first order of the Magnus expansion [26].

Acknowledgments

G. S. Boutis acknowledges support by Award Number SC1GM086268 from the National Institute Of General Medical Sciences. The content is solely the responsibility of the authors and does not necessarily represent the official views of the National Institute Of General Medical Sciences or the National Institutes of Health.

References

[1] H. Shinar, G. Navon, Multinuclear NMR and microscopic MRI studies of the articular cartilage nanostructure, NMR Biomed. 19 (2006) 877–893.
[2] Y. Sharf, T. Knubovets, D. Dayan, A. Hirshberg, S. Akselrod, G. Navon, The source of NMR-detected motional anisotropy of water in blood vessel walls, Biophys. J. 73 (1997) 1198–1204.
[3] U. Eliav, G. Navon, A study of dipolar interaction and dynamic processes of water molecules in tendon by ^{1}H and ^{2}H homonuclear and heteronuclear multiple-quantum-filtered NMR spectroscopy, J. Magn. Reson. 137 (1999) 295–310.
[4] L. Frish, N. Friedman, M. Sheves, Y. Cohen, The interaction of water molecules with purple membrane suspension using ^{2}H double-quantum filter, ^{1}H and ^{2}H diffusion nuclear magnetic resonance, Biopolymers 75 (2004) 46–59.
[5] Y. Sharf, U. Eliav, H. Shinar, G. Navon, Detection of anisotroscopy in cartilage using ^{2}H double-quantum-filtered NMR-spectroscopy, J. Magn. Reson. Ser. B 107 (1994) 60–767.
[6] H. Shinar, Y. Seo, K. Ikoma, Y. Kusaka, U. Eliav, G. Navon, Mapping the fiber orientation in articular cartilage at rest and under pressure studied by ^{2}H double quantum filtered MRI, Magn. Reson. Med. 48 (2002) 322–330.
[7] H. Shinar, Y. Seo, G. Navon, Discrimination between the different compartments in sciatic nerve by ^{2}H double-quantum-filtered NMR, J. Magn. Reson. 129 (1997) 98–104.
[8] W. Perea, M. Cannella, J. Yang, A.J. Vega, T. Polenova, M. Marcolongo, ^{2}H double quantum filtered (DQF) NMR spectroscopy of the nucleus pulposus tissues of the intervertebral disc, Magn. Reson. Med. 57 (2007) 990–999.
[9] G. Navon, H. Shinar, U. Eliav, Y. Seo, Multiquantum filters and order in tissues, NMR Biomed. 14 (2001) 112–132.
[10] G. Bodenhausen, H. Kogler, R.R. Ernst, Selection of coherence-transfer pathways in NMR pulse experiments, J. Magn. Reson. 58 (1984) 370–388.
[11] G. Bodenhausen, R.L. Vold, R.R. Vold, Multiple quantum spin-echo spectroscopy, J. Magn. Reson. 37 (1980) 93–106.
[12] J. Cavanagh, W.J. Faribrother, A.G. Palmer III, N.J. Skelton, Protein NMR Spectroscopy: Principles and Practice, Academic Press, 1995. pp. 177–178.
[13] G. Bodenhausen, R. Freeman, G.A. Morris, D.L. Turner, NMR spectra of some simple spin systems studied by two-dimenstional Fourier transformation of spin echoes, J. Magn. Reson. 31 (1978) 75–95.
[14] N. Murali, Y.V.S. Ramakrishna, K. Chandrasekhar, M.A. Thomas, A. Kumar, Flip angle dependence in two-dimensional multiple quantum coherence NMR spectroscopy, Pramana 23 (1984) 547–557.
[15] A. Jerschow, Nonideal rotations in nuclear magnetic resonance: estimation of coherence transfer leakage, J. Chem. Phys. 113 (2000) 979–986.
[16] C. Matthies, A.M. Nagel, L.R. Schad, P. Bachert, Reduction of B_0 inhomogeneity effects in triple-quantum-filtered sodium imaging, J. Magn. Reson. 202 (2010) 239–244.
[17] C.F.-Y. Chuang, NMR multiple quantum filters via RF gradients, Ph.D. Thesis, Massachusetts Institute of Technology, 1994.
[18] J. Baum, M. Munowitz, A.N. Garroway, A. Pines, Multiple-quantum dynamics in solid state NMR, J. Chem. Phys. 83 (1985) 2015–2025.
[19] M.H. Levitt, Spin Dynamics: Basics of Nuclear Magnetic Resonance, John Wiley and Sons Ltd., 2001. pp. 201–202.
[20] A. Jerschow, From nuclear structure to the quadrupolar NMR interaction and high-resolution spectroscopy, Prog. Nuc. Magn. Reson. Spec. 46 (2005) 63–78.
[21] S. Vega, A. Pines, Operator formalism for double quantum NMR, J. Chem. Phys. 66 (1977) 5624–5644.
[22] B.C. Gerstein, C.R. Dybowski, Transient Techniques in NMR of Solids: An Introduction of Theory and Practice, Academic Press, 1985. pp. 215–220.
[23] S. Berger, S. Braun, 200 and More NMR Experiments, WILEY-VCH, 2004. pp. 89–90.
[24] A.J. Vega, Controlling the effects of pulse transients and RF inhomogeneity in phase-modulated multiple-pulse sequences for homonuclear decoupling in solid-state proton NMR, J. Magn. Reson. 170 (2004) 22–41.
[25] W.K. Rhim, D.D. Elleman, L.B. Schreiber, R.W. Vaughan, Analysis of multiple pulse NMR in solids. II, J. Chem. Phys. 60 (1974) 4595–4604.
[26] U. Haeberlen, Advances in Magnetic Resonance. Suppl. 1, Academic Press, 1976.